The line flux from the SNR can be translated into an ejected mass of ^{44}Ti, if we know the age and distance of the SNR. Recent measurements of the ^{44}Ti lifetime (see refs 18, 19, and references therein) were used to derive a weighted mean of 90.4 ± 1.3 years. We note that the effective ^{44}Ti lifetime in SNRs could be larger, depending on the degree of ionization of the ^{44}Ti and its Lorentz factor. The derived value of the ejected ^{44}Ti mass is mainly sensitive to the actual value of the lifetime and is less critically dependent on the distance to, and the age of, the SNR.

The parameters (age and distance) are not available from the γ-ray measurements alone. Fortunately however, a possible counterpart of the newly discovered SNR was recently (independently) detected in Rosat data[20]: an extended feature of ~2° diameter centred at Galactic longitude $l = 266.3°$, latitude $b = 1.2°$ only 0.4° away from the ^{44}Ti excess, well within the measurement uncertainties.

By combining the γ-ray line flux and the X-ray diameter[20] with an assumed typical ^{44}Ti yield of $\sim 5 \times 10^{-5} M_{\odot}$ for supernovae of different types[6–9], and taking as representative an expansion velocity of ~5,000 km s^{-1} (ref. 21) for the supernova ejecta, we derive a distance of ~200 pc, and an age of the SNR of ~680 yr. For larger ^{44}Ti yields and larger expansion velocities, the distance estimate becomes larger and the age estimate becomes less. We note that the SNR expansion velocity, when evaluated from the SNR X-ray spectrum[20], has the same value of ~5,000 km s^{-1}.

We can only speculate about the reasons why this supernova was not observed ~700 years ago: we can consider the possible existence both of optically subluminous supernovae[22] and of absorbing material in front of the supernova. In addition, the celestial position and the time of the event might have been unfavourable for an observation. Information about the existence and type of the compact stellar-like remnant of the supernova, and the elemental abundances of the SNR, will have to await future optical, radio, X-ray and γ-ray measurements. □

Received 3 April; accepted 20 August 1998.

1. van den Bergh, S. & Tammann, G. A. Galactic and extragalactic supernova rates. *Annu. Rev. Astron. Astrophys.* **29,** 363–407 (1991).
2. Ashworth, W. B. A probable Flamsteed observation of the Cassiopeia supernova. *J. Hist. Astron.* **11,** 1–14 (1980).
3. Strom, R. G. "Guest Stars", sample completeness and the local supernova rate. *Astron. Astrophys.* **288,** L1–L4 (1994).
4. Iyudin, A. F. *et al.* COMPTEL observations of ^{44}Ti gamma-ray line emission from Cas A. *Astron. Astrophys.* **284,** L1–L4 (1994).
5. Iyudin, A. F. *et al.* in *Proc. 2nd INTEGRAL Workshop* 37–41 (SP-382, ESA, 1997).
6. Nomoto, K., Thielemann, F.-K. & Yokoi, K. Accreting white dwarfs models for type I supernovae. III. Carbon deflagration supernovae. *Astrophys. J.* **286,** 644–658 (1984).
7. Woosley, S. E. & Weaver, T. A. The evolution and explosion of massive stars. II. Explosive hydrodynamics and nucleosynthesis. *Astrophys. J. Suppl.* **101,** 181–235 (1995).
8. Thielemann, F.-K., Nomoto, K. & Hashimoto, M. A. Core-collapsed supernovae and their ejecta. *Astrophys. J.* **460,** 408–436 (1996).
9. Woosley, S. E. & Weaver, T. A. Sub-Chandrasekhar mass models for type Ia supernovae. *Astrophys. J.* **423,** 371–379 (1994).
10. Clayton, D. D., Colgate, S. A. & Fishman, G. J. Gamma-ray lines from young supernova remnants. *Astrophys. J.* **155,** 75–82 (1969).
11. Dupraz, C. *et al.* COMPTEL three-year search for galactic sources of ^{44}Ti gamma-ray line emission at 1.167 MeV. *Astron. Astrophys.* **324,** 683–689 (1997).
12. Schönfelder, V. *et al.* Instrument description and performance of the imaging gamma-ray telescope COMPTEL aboard the Compton Gamma-Ray Observatory. *Astrophys. J. Suppl.* **86,** 657–692 (1993).
13. Knödlseder, J. *The Origin of ^{26}Al in the Galaxy.* Thesis, Toulouse Univ. (1997).
14. van Dijk, R. *Gamma-ray Observations of X-Ray Binaries with COMPTEL.* Thesis, Toulouse Univ. (1996).
15. Oberlack, U. *Über die Natur der Galaktischen ^{26}Al-Quellen Untersuchung des 1.8-MeV-Himmels mit COMPTEL.* Thesis, München Techn. Univ. (1997).
16. Diehl, R. *et al.* 1.809 MeV gamma-rays from the Vela region. *Astron. Astrophys.* **298,** L25–L28 (1995).
17. Oberlack, U. *et al.* Implications of the ^{26}Al emission of 1.8 MeV from the Vela region. *Astrophys. J. Suppl.* **92,** 433–439 (1994).
18. Norman, E. B. *et al.* Half-life of ^{44}Ti. *Phys. Rev. C.* **57,** 2010–2016 (1998).
19. Görres, J. *et al.* Lifetime of ^{44}Ti as probe for supernova models. *Phys. Rev. Lett.* **80,** 2554–2557 (1998).
20. Aschenbach, B. Discovery of a young nearby supernova remnant. *Nature* **396,** 141–142 (1998).
21. Weaver, T. A. & Woosley, S. E. in *AIP Conf. Proc. 63: Supernovae Spectra* (eds Meyerott, R. & Gillespie, G. H.) 15–37 (AIP, New York, 1980).
22. Schaefer, B. E. Volume-limited sample of supernovae. *Astrophys. J.* **464,** 404–411 (1996).

Acknowledgements. We thank the COMPTEL team for their support. A.F.I. acknowledges support from the German Bundesministerium für Bildung, Wissenschaft, Forschung und Technologie.

Correspondence and requests for materials should be addressed to A.F.I. (e-mail: ani@mpe-garching.mpg.de).

Paramagnetic Meissner effect in small superconductors

A. K. Geim*, S. V. Dubonos†, J. G. S. Lok*, M. Henini‡ & J. C. Maan*

* *Research Institute for Materials, University of Nijmegen, 6525 ED Nijmegen, The Netherlands*
† *Institute for Microelectronics Technology, Russian Academy of Sciences, 142432 Chernogolovka, Russia*
‡ *Department of Physics, University of Nottingham, Nottingham NG7 2RD, UK*

A superconductor placed in a magnetic field and cooled down through the transition temperature expels magnetic flux. This phenomenon, known as the Meissner effect, is arguably the most essential property of superconductors and implies zero resistivity. Surprisingly, several recent experiments have shown that some superconducting samples[1–7] may attract magnetic field—the so-called paramagnetic Meissner effect. The scarce, if not controversial, experimental evidence for this effect makes it difficult to identify the origin of this enigmatic phenomenon, although a large number of possible explanations have been advanced[8–16]. Here we report observations of the paramagnetic Meissner effect with a resolution better than one quantum of magnetic flux. The paramagnetic Meissner effect is found to be an oscillating function of the magnetic field (due to flux quantization) and replaces the normal Meissner effect only above a certain field when several flux quanta are frozen inside a superconductor. The paramagnetic state is found to be metastable and the Meissner state can be restored by external noise. We conclude that the paramagnetic Meissner effect is related to the surface superconductivity and, therefore, represents a general property of superconductors: on decreasing temperature, the flux captured at the third (surface) critical field inside the superconducting sheath compresses into a smaller volume, allowing extra flux to penetrate at the surface.

The evidence for the paramagnetic Meissner effect (PME) in high-temperature superconductors[1–5] has prompted the appearance of a number of theories attributing the effect to a non-conventional superconductivity in these materials[8–13]. Although it is possible that the proposed mechanisms do play a role in high-T_c superconductors[17], more recent observations of PME in Nb (refs 6, 7) clearly indicate the existence of another, less-exotic mechanism: the limited choice of assumptions in this case makes the origin of PME more mysterious. To explain PME in terms of conventional superconductivity, theory employs the idea of flux capture inside a superconducting sample and its consequent compression with decreasing temperature[14–16]. The flux capture can be caused by inhomogeneities[14,15] but, in principle, could also be an intrinsic property of any finite-size superconductor due to the presence of the sample boundary[16].

Here we attempt to elucidate the origin of PME by studying small (micrometre-size) superconducting disks. Confinement of superconductivity in a small volume, comparable to the characteristic superconducting lengths λ and ξ, leads to pronounced quantization, so that a mesoscopic superconductor resides in one of a series of well-resolved states, depending on temperature and magnetic field. These superconducting states are characterised by a different number and distribution of vortices[18–21]. In comparison with the previous studies of PME on macroscopic (centimetre-size) disks, the small size of our samples gives the advantage that we can measure magnetization of individual vortex states. In addition, our samples behave very much like ideal superconductors: in the context of this work, it is important that they clearly exhibit surface superconductivity and no noticeable pinning[18–20]. That they act in this way is probably due to their small size.

Magnetization was measured by ballistic Hall magnetometers that work as fluxmeters with a detection loop of $\sim 1\,\mu m^2$ (ref. 22). The technique has a resolution of $\sim 10^4$ Bohr magnetons and is still the only technique allowing studies of individual mesoscopic superconductors below the transition temperature T_c. We have studied a number ($\sim$20) of superconducting disks made from Al and Nb with diameters from 0.3 to 3 μm and thicknesses t from 0.03 to 0.15 μm, using magnetometers of various widths from 1 to 2.5 μm. The behaviour described below is reproducible for identical samples and changes consistently with changing the sample parameters.

Figure 1 shows a representative set of magnetization curves measured for a 2.5-μm-diameter Al disk on cooling it down in different magnetic fields H (so-called field-cooling (FC) regime). In low fields, we observe the normal (negative) Meissner response, and below 10 G the magnetization curves are practically identical. In intermediate fields, the sign of the Meissner effect oscillates between positive and negative, depending on the particular field value, while in higher fields it stays positive, until the superconductivity is destroyed above 140 G. The detailed field dependence of the Meissner effect is shown in Fig. 2, which plots the low-temperature value of the FC magnetization (deduced from curves such as those in Fig. 1) for Al disks of diameter 1.0 and 2.5 μm. The strongly oscillating behaviour clearly seen for the larger sample is due to size quantization. Each jump corresponds to a change in the number of vortices inside the disk, which can either form an array of single-quantum vortices or assemble into a single giant vortex[16,18–21]. The latter configuration is generally expected at fields between the second and third critical fields, $H_{c2} < H < H_{c3}$, that is, it corresponds to the surface superconductivity in a confined geometry. The smaller sample does not exhibit this rapidly oscillating field dependence, and its Meissner response remains negative over the entire field interval. Such qualitatively different behaviour is related to the fact that, in the smaller sample, the superconductivity is suppressed by $\sim$3 flux quanta, ϕ_0, entering the disk area while $\sim 20\phi_0$ are necessary to destroy superconductivity of the larger disk[18–20].

To summarize the behaviour observed on other samples: we always found a diamagnetic response in low magnetic fields which gives way to a paramagnetic response only after the entry of at least several flux quanta into the disk interior, provided that the superconductivity survives to such fields (compare the two samples in Fig. 2). This seems to be in contrast to the previous studies on macroscopic samples, where the PME was normally found in very low fields and gradually disappeared with increasing field. However, one should take into account that even the lowest fields in the previous experiments allowed many thousands of flux quanta inside the sample interior. We also observe that, with decreasing disk thickness, the reversal of the sign of the Meissner effect tends to occur at lower fields and the PME magnitude becomes larger. No qualitative difference in behaviour is observed between disks of circular and square shapes.

The origin of the PME becomes evident if we compare the field dependence of the Meissner effect discussed above with the magnetization response measured by sweeping the magnetic field at a constant temperature (CT regime) (Fig. 3). Instead of a single magnetization curve characteristic of macroscopic superconductors, the spatial confinement gives rise to a family of magnetization curves corresponding to different vortex states. Several superconducting states can be realised at the same applied field (up to five as seen in Fig. 3) but only the state with the most negative CT magnetization is thermodynamically stable[19,20]. Other states are metastable and become observable due to the presence of the surface (Bean–Livingston) barrier[18–21]. Recent theory[19,20] is in good agreement with the similar CT curves reported previously[18].

Figure 3 clearly shows that the paramagnetic states reached via field cooling are all metastable. Indeed, the FC data predictably fall on the CT curves because only these distributions of the order

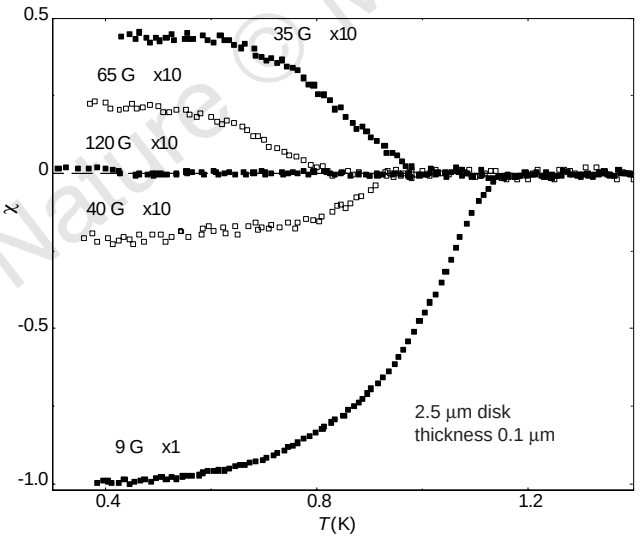

Figure 1 Magnetic susceptibility χ of an aluminium disk for various magnetic fields perpendicular to the disk surface. There is no hysteresis when sweeping the temperature up and down. Magnetization amplitude is normalized to its value at low fields (<5 G) at 0.3 K. The top curves are multiplied by a factor of 10. At 0.3 K, the bulk critical field H_{c2} for this Al film is $\sim$80 G (measured resistively); surface critical field $H_{c3} \approx 140$ G (magnetization data); $T_c \approx 1.25$ K; $\lambda(0) \approx 70$ nm; Ginzburg–Landau parameter $\kappa = \lambda/\xi \approx 0.3$.

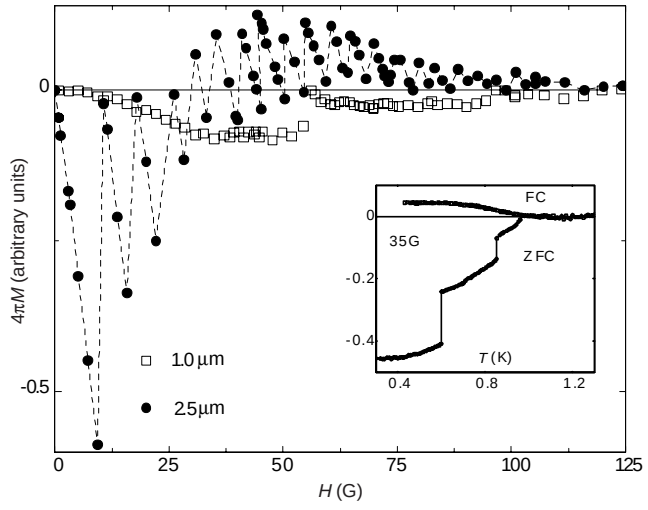

Figure 2 Detailed field dependence of the Meissner response. The figure plots the magnetic flux captured inside or expelled out of a Hall magnetometer of 2.5 μm width at 0.4 K, due to the presence of superconducting disks ($\Delta\Phi = \langle B \rangle - H = 4\pi M$; ref. 22). The two disks were fabricated simultaneously by thermal evaporation and differ only in their diameters. The dashed line is a guide to the eye. The inset compares FC and zero-field-cooling (ZFC) magnetization. In the latter case, the sample is cooled down in zero field, then a field is applied and the magnetization is measured as temperature increases. The inset is for the 2.5-μm disk at the field where the paramagnetic response is close to its maximum value. The ZFC response is always diamagnetic. The jumps in the ZFC curve correspond to entry of individual vortices into the disk interior.

parameter are allowed by quantization. However, among all possible states at a given field, the system unexpectedly 'chooses' the metastable state with the most positive possible magnetization. Only if we remove the proper screening in our experimental setup does a metastable high-magnetization state eventually relax to the corresponding stable state on the lowest curve. The same result was obtained when the experiment was carried out in a more controllable manner, by applying an oscillating magnetic field at a constant H. One can verify that, according to Fig. 3, an oscillating (fluctuating) field moves the system down the ladder of curves, towards equilibrium.

How, on cooling down, the system can end up in the most thermodynamically unfavourable state may be seen from the following consideration. Superconducting states in a confined geometry can be characterised by a quantum number L corresponding to the number of nodes in the distribution of the complex order parameter Ψ along the sample circumference. For the case of a giant vortex and an array of single-quantum vortices, L has a simpler meaning: it is the angular momentum and the number of vortex cores, respectively[18–25]. Transitions between states with different L are of first order and lead to jumps in magnetization (for example, see Fig. 3 and Fig. 2 inset)[19,20,25]. The FC curves of Fig. 1 do not exhibit any magnetization jumps; further analysis of our experimental data shows that no jumps between different L occur at temperatures as little as 0.03 K away from the superconducting transition that on our curves corresponds to H_{c3} (refs 18–20). This proves that, on cooling down, the superconducting system preserves its L-fold symmetry as it was initially induced by the surface superconductivity at H_{c3} in the form of a giant vortex.

It is this persistence of L down to low temperatures that is responsible for the PME. We now describe a simple model, which combines the ideas of refs 14 and 16, that explains the essential physics involved. Close to H_{c3}, the magnetic field is distributed homogeneously and it requires the 'high-temperature' magnetic flux $\Phi_{HT} \approx \phi_0(L + L^{1/2})$ (ref. 24) to initiate a giant vortex with momentum L inside a superconducting disk of radius r. As the temperature decreases below the surface superconducting transition, the superconducting sheath at the disk perimeter rapidly expands inside, compressing the giant vortex into a small volume (see Fig. 3 inset; we consider the case $\lambda \ll r$). The compressed flux inside a giant vortex is equal to $\phi_0 L$, that is, Φ_{HT} is practically conserved for $L \gg 1$. When at H_{c2} the giant vortex spits into L single-quantum vortices, the captured flux changes little[20]. At this point, we have to take into account the fact that the magnetic field also penetrates at the disk boundary, giving rise to an additional flux through the disk of the order of $\pi r \lambda H_B$, where H_B is the field strength in the λ-layer at the surface. The magnetization response is paramagnetic if the low-temperature value of the total flux, $\Phi_{LT} \approx \phi_0 L + \pi r \lambda H_B$, is larger than Φ_{HT}. For a superconducting cylinder, $H_B = H$ and the PME appears at relatively large $L > (r/\lambda)^2$ and its amplitude is rather small ($\mu \approx \lambda/r$).

The plate geometry significantly enhances the PME because H_B is increased by demagnetization effects[14]. If the central region occupied by a vortex or vortices is small compared to the disk area, one can approximate $H_B \approx H(r/t)$. This yields the paramagnetic response $\mu \approx \lambda/t$, considerable even for macroscopic thin disks. The plate geometry also leads to an earlier start of PME. This model is in good, semi-quantitative agreement with the behaviour observed in our experiment, and also explains the PME in macroscopic Nb disks[6,7] and, possibly, in high-T_c superconductors. The latter often consist of micrometre-size grains or, owing to inhomogeneity of single crystals, can effectively mimic such a medium. □

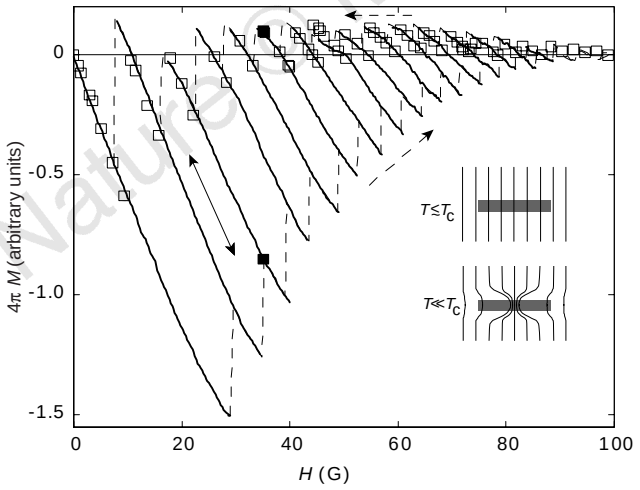

Figure 3 Comparison of the magnetization states reached by cooling in a field and by sweeping the field at a constant temperature. The field-cooling (FC) data shown by open squares are for the 2.5-μm disk of Fig. 2. The lines are for the CT regime. The solid curves were measured by pausing at various fields and then sweeping the field up and down (0.4 K). When the magnetic field is swept continuously, the magnetization evolves along one of the solid curves until it reaches the end of this curve and jumps to the next one, belonging to another vortex state. Then, the process repeats itself all over again as shown by dashed lines. Arrows show the direction of the sweep. The filled squares at 35 G indicate the low-temperature states for the FC and ZFC curves of Fig. 2. The inset illustrates the compression of a giant vortex (T close but below T_c) into a smaller volume (T further away from T_c) which allows extra flux to enter the sample at the surface.

Received 22 June; accepted 24 August 1998.

1. Braunisch, W. *et al.* Paramagnetic Meissner effect in Bi high-temperature superconductors. *Phys. Rev. Lett.* **68,** 1908–1911 (1992).
2. Schliepe, B., Stindtmann, M., Nikolic, I. & Baberschke, K. Positive field-cooled susceptibility in high-T_C superconductors. *Phys. Rev. B* **47,** 8331–8334 (1993).
3. Heizel, C., Theiling, T. & Zieman, P. Paramagnetic Meissner effect analyzed by 2nd harmonics of the magnetic susceptibiity. *Phys. Rev. B* **48,** 3445–3454 (1993).
4. Magnusson, J. *et al.* Time-dependence of the magnetization of BiSrCaCuO displaying the paramagnetic Meissner effect. *Phys. Rev. B* **52,** 7675–7681 (1995).
5. Riedling, S. *et al.* Observation of the Wohlleben effect in YBaCuO single crystals. *Phys. Rev. B* **49,** 13283–13286 (1994).
6. Thompson, D. J., Minhaj, M. S. M., Wenger, L. E. & Chen, J. T. Observation of paramagnetic Meissner effect in niobium disks. *Phys. Rev. Lett.* **75,** 529–532 (1995).
7. Kostic, P. *et al.* Paramagnetic Meissner effect in Nb. *Phys. Rev. B* **53,** 791–801 (1996).
8. Sigrist, M. & Rice, T. M. Paramagnetic effect in High-T_C superconductors—a hint for d-wave superconductivity. *J. Phys. Soc. Jpn* **61,** 4283–4286 (1992).
9. Kusmartsev, F. V. Destruction of the Meissner effect in granular high-temperature superconductors. *Phys. Rev. Lett.* **69,** 2268–2271 (1992).
10. Dominguez, D., Jagla, E. A. & Balseiro, C. A. Phenomenological theory of the paramagnetic Meissner effect. *Phys. Rev. Lett.* **72,** 2773–2776 (1994).
11. Khomskii, D. Wohlleben effect (paramagnetic Meissner effect) in high-temperature superconductors. *J. Low Temp. Phys.* **95,** 205–223 (1994).
12. Chen, D. X. & Hernando, A. Paramagnetic Meissner effect and pi Josephson junctions. *Europhys. Lett.* **26,** 365–370 (1994).
13. Shrivastava, K. N. Para-Meissner oscillations in the magnetization of a high-temperature superconductor. *Phys. Lett. A* **188,** 182–186 (1994).
14. Koshelev, A. E. & Larkin, A. I. Paramagnetic moment in field-cooled superconducting plates—paramagnetic Meissner effect. *Phys. Rev. B* **52,** 13559–13562 (1995).
15. Khalil, A. E. Inversion of Meissner effect and granular disorder in BiSrCaCuO superconductors. *Phys. Rev. B* **55,** 6625–6630 (1997).
16. Moshchalkov, V. V., Qui, X. G. & Bruyndoncz, V. Paramagnetic Meissner effect from the self-consistent solution of the Ginzburg–Landau equations. *Phys. Rev. B* **55,** 11793–11801 (1997).
17. Rice, T. M. & Sigrist, M. Paramagnetic Meissner effect in Nb—Comment. *Phys. Rev. B* **55,** 14647–14848 (1997).
18. Geim, A. K. *et al.* Phase transitions in individual sub-micrometre superconductors. *Nature* **390,** 259–262 (1997).
19. Schweigert, V. A. & Peeters, F. M. Phase transitions in thin superconducting disks. *Phys. Rev. B* **57,** 13817–13832 (1998).
20. Schweigert, V. A., Peeters, F. M. & Deo, P. S. Vortex phase diagram for mesoscopic superconducting disks. *Phys. Rev. Lett.* **81,** 2783–2786 (1998).
21. Bolech, A. C., Buscaglia, G. C. & Lopez, A. Numerical simulation of vortex arrays in thin superconducting films. *Phys. Rev. B* **52,** 15719–15722 (1995).
22. Geim, A. K. *et al.* Ballistic Hall micromagnetometry. *Appl. Phys. Lett.* **71,** 2379–2381 (1997).
23. Bezryadin, A., Buzdin, A. & Pannetier, B. Phase diagram of multiply connected superconductors. *Phys. Rev. B* **51,** 3718–3724 (1995).
24. Benoist, R. & Zwerger, W. Critical fields of mesoscopic superconductors. *Z. Phys. B* **103,** 377–381 (1997).
25. Palacios, J. J. Vortex matter in superconducting mesoscopic disks: structure, magnetization, and phase transitons. *Phys. Rev. B,* **58,** R5948–R5951 (1998).

Acknowledgements. We thank I. V. Grigorieva, V. V. Moschalkov and F. M. Peeters for discussions and FOM for financial support.

Correspondence and requests for materials should be addressed to A.K.G. (geim@sci.kun.nl).